Original Article

Predicting radiation pneumonitis with fuzzy clustering neural network using 4DCT ventilation image based dosimetric parameters

Peng Huang, Hui Yan, Zhihui Hu, Zhiqiang Liu, Yuan Tian, Jianrong Dai

Department of Radiation Oncology, National Cancer Center/National Clinical Research Center for Cancer/Cancer Hospital, Chinese Academy of Medical Sciences and Peking Union Medical College, Beijing, China

Correspondence to: Yuan Tian; Jianrong Dai. Department of Radiation Oncology, National Cancer Center/National Clinical Research Center for Cancer/Cancer Hospital, Chinese Academy of Medical Sciences and Peking Union Medical College, Beijing, China.
Email: yuan.tian@cicams.ac.cn; dai_jianrong@cicams.ac.cn.

Background: To develop a fuzzy clustering neural network to predict radiation-induced pneumonitis (RP) using four-dimensional computed tomography (4DCT) ventilation image (VI) based dosimetric parameters for thoracic cancer patients.

Methods: The VI were retrospectively calculated from pre-treatment 4DCT data using a deformable image registration (DIR) and an improved VI algorithm. Similar to dose-volume histogram (DVH) of intensity modulated radiotherapy (IMRT), dose-function histogram (DFH) was derived from dose distribution and VI. Then, the dose-function metrics were calculated from DFH. For comparison, the dose-volume metrics were calculated from DVH. Correspondingly, two sets of feature vectors were formed from the dose-volume metrics and the dose-function metrics, respectively. For the feature vectors of each set, they were first pre-processed by principal component analysis (PCA) to reduce feature dimensions. Then, they were grouped to few clusters determined by fuzzy c-means (FCM) algorithm. Next, the neural network was trained to correlate the dosimetric parameters with RP based on the feature vectors of each cluster. Finally, the occurrence of RP was predicted by the neural network on the test data.

Results: Through PCA analysis, the top 5 principal components were selected. Their contribution is more than 98%, which is adequate to represent the original feature space of input data. Based on the clustering validity indexes, the optimal number of clusters is 4 and used for subsequent fuzzy clustering of the input data. After network training, the areas under the curve (AUC) of the prediction model is 0.77 using VI-based dosimetric parameters and 0.67 using structure-based dosimetric parameters.

Conclusions: Compared to the structure-based dosimetric features, the VI-based dosimetric features are more relevant to lung function and presented higher prediction accuracy of RP. The fuzzy clustering neural network improved the prediction accuracy of RP compared to the conventional neural network. The combination of VI-based dose-function metrics and fuzzy clustering neural network provides an effective predictive model for assessing lung toxicity risk after radiotherapy.

Keywords: Fuzzy clustering; neural network; four-dimensional computed tomography (4DCT); ventilation image (VI); radiation-induced pneumonitis (RP)

Submitted Sep 25, 2020. Accepted for publication Mar 05, 2021.
doi: 10.21037/qims-20-1095
View this article at: http://dx.doi.org/10.21037/qims-20-1095

Introduction

Radiation pneumonitis (RP) is a type of irreversible lymphocytic alveolar inflammation, which usually occurs 1–6 months after radiotherapy with symptoms of dry cough, low-grade fever, and dyspnea. Severe radiation pneumonitis can lead to extensive fibrosis of the lung and damage of

respiratory function. It affects the life quality of patients after radiotherapy and even endanger patient life. It is also the main factor in restricting the dose escalation of radiotherapy dose (1,2). The incidence of RP was 5–50% and the mortality was as high as 50%. At present, there is no specific treatment for radiation pneumonitis and pulmonary fibrosis after radiotherapy. How to avoid and reduce the occurrence of RP is one of the important parts in thoracic radiotherapy. The establishment of an effective RP prediction model can reflect the risk of RP to a certain extent, which is of great clinical significance to prevent RP (3,4).

Current research suggests that dosimetric metrics have important predictive value for RP. The occurrence and severity of RT-induced pulmonary injury is closely related to the volume of lung irradiated. Numerous studies have attempted to identify features that correlate with RP. Dosimetric metrics that describe features of the spatial dose distribution have been already reported to correlate with the development of RP (5-9). However, an agreement has not been reached about which of these dose-volume metrics should be used to predict the risk of RP (10). In addition to the structure-based dosimetric metrics, there is another type of dosimetric metric extracted from the functional images such as perfusion image and ventilation image (VI). Single photon emission computed tomography (SPECT), positron emission computed tomography (PET), and magnetic resonance (MR) imaging have been used as functional imaging techniques for radiation therapy for many years and potentially provide information on perfusion in addition to ventilation (11-13). However, these functional imaging techniques require additional costs and time which is more expensive in clinic.

Recently, a new technique for ventilation imaging using four-dimensional computed tomography (4DCT) with deformable image registration (DIR) has been investigated (14,15). In clinic, 4DCT images are usually acquired for lung cancer patients to allow a higher accurate contouring of the target volume with respiratory motion. The 4DCT ventilation imaging technique can be used for treatment planning, allowing ventilation imaging to be obtained without the additional costs and time of other functional imaging modalities (16). The 4DCT ventilation information can be calculated using DIR performed from the peak-exhale and peak-inhale images. The 4DCT-based VI has been used to assess the functional changes in lung tissue (17-20), assess lung toxicity risk (14,21), and in guiding the planning of radiotherapy treatments (22-26).

Currently, the following three calculation algorithms have been proposed for 4DCT VI image: (I) the density-based algorithm which determines the ventilation in term of Hounsfield Unit (HU) change corresponding to inhalation and exhalation breathing phases (27); (II) the Jacobian-based algorithm which derives the ventilation from the Jacobian determinant of the deformable vector field (28); and (III) the regional-based algorithm which estimates the ventilation in terms of the 4D time-averaged regional product of air and tissue densities at each voxel (29). However, the correlation between the VIs resulted by these algorithms and the clinical gold standards, including [^{99m}Tc-SPECT (30) and ^{68}Ga-Galligas PET (31)], are highly variable (32). Several investigations applied dose-function metrics for treatment planning and evaluation. Studies have shown that dose-function metrics are more predictive of radiation toxicity than dose alone (33-35). In our previous study, a simplified regional-based VI generation algorithm was proposed, which only requires the average 4DCT as input and is more accurate and computational efficiency comparing to the other three algorithms (36). It is unclear whether it would also provide better dose-function metrics for evaluating the risk of radiation-induced lung toxicity.

Numerous linear or non-linear classifiers in the field of pattern recognition and intelligent controlling have been proposed over the past decades. Among them, the feed-forward neural network has been used mostly as a predictive model for evaluating RP risk (37-39). The traditional feed-forward neural network algorithm has a strong learning ability but suffers from slow convergence and overfitting of model. To overcome this, feature selection (40), such as principal components analysis (PCA), was introduced in this study to reduce the dimensionality of feature space and to enhance the performance of predictive model. In addition, unsupervised learning (41,42), such as clustering, was used to group samples into different clusters before they proceeded to the predictive model. This enhanced the similarity of features within each cluster and improved the efficiency of supervised learning.

In this study, a hybrid neural network was proposed and used as a primary prediction model for correlating dose-function metrics generated by the simplified regional-based algorithm with the occurrence of RP. PCA was employed to reduce the feature vector to few dimensions. The fuzzy c-means (FCM) method was used to group samples into few clusters according to the unsupervised learning. Then the feed-forward neural network was trained on the samples of each cluster to learn the correlation between (structure-

based or ventilation-based) dosimetric parameters and category labels. The performance of the neural network based on structure-based and ventilation-based dosimetric parameters was evaluated. The rest of this paper is organized as follows. In Section Methods, the generation of VI and dose-function formulation was described at first. Then the principles of PCA and FCM were explained in detail. Later, the prediction model and evaluation methods were introduced. In section Results, the prediction accuracy of hybrid neural network with respect to the two types of dosimetric metrics was presented. Finally, the advantages and disadvantages of the ventilation-based dosimetric metric and hybrid neural network were discussed in section Discussion.

Methods

Clinical data

A total of 244 patients with lung cancer who underwent intensity-modulated radiotherapy (IMRT) and 4DCT simulation from January 2015 to January 2018 were enrolled in this study, including 171 males and 73 females, aged 40–78 years. All patients were followed up for more than 6 months after completion of radiotherapy. Symptoms of radiation pneumonitis were recorded according to the common toxicity criteria of adverse events (CTCAE), version 4.03. According to this classification, the clinical data was divided into two groups, namely RP group (≥3 grade) and No-RP group (≤2 grade). All patients were planned using Pinnacle treatment planning system (Version 9.0, Philips Radiation Oncology Systems). IMRT or VMAT plans were designed for each patient. A total of 95% of target volume should be encompassed by 95% of the prescribed dose.

4DCT-based VI

Free-breathing 4DCT was acquired with patients in a supine position using a Brilliance Bigbore CT scanner (Philips Healthcare, Andover, MA) with no i.v. contrast. For each patient, 4DCT images of the entire target and thorax, as well as upper abdomen were obtained. Real-time Positioning Management (RPM, Varian Medical Systems, Palo Alto, CA) was used for respiratory monitoring. The entire respiratory cycle was recorded and divided into ten equal temporal phases, defining the peak inhalation phase as T00 and peak-exhalation phase as T50 (29). The raw data was sorted into corresponding phase bins and reconstructed into ten phase CT datasets (T00-T90, respectively) with the dimension of 512×512 and 5 mm slice thickness. Average CT was reconstructed from 10-phase 4DCT data with respect to the percentage of time in the same spatial resolution.

The lung volume was contoured on each CT phase using threshold-based approach with intensity cutoff between –250 and –1,000 HU in MIMvista. Central airway and great vessels where the ^{99m}Tc-Technegas physiologically concentrated were manually trimmed to define the region of interest for comparison. The lung volume was transformed into a 3D binary mask in which the value of voxel inside and outside the lung was set equal to 1 and 0, respectively. Binary lung masks, ten phases of 4DCT (T00, …, T90) and average CTs were saved as matrices using an in-house developed image toolkit called FLICT (i.e., functional lung image based on 4DCT) on MATLAB (Mathworks Inc.).

The ventilation was originally estimated by the regional-based algorithm in terms of 4D time-averaged regional product of air and tissue densities at each voxel (29) as below.

$$\begin{aligned} CTVI_{HU}(x) &= \sum_{\varnothing=1}^{N} v_{\varnothing}(x)/N \ , \ \text{where} \\ v_{\varnothing}(x) &= \begin{cases} f_{\varnothing}^{Air}(x)\times f_{\varnothing}^{Tissure}(x) & if\ x\in L_{\varnothing} \\ 0 & if\ x\notin L_{\varnothing} \end{cases} \\ &= \begin{cases} \dfrac{HU_{\varnothing}(X)}{-1000}\times\dfrac{HU_{\varnothing}(X)+1000}{1000} & if\ x\in L_{\varnothing} \\ 0 & if\ x\notin L_{\varnothing} \end{cases} \end{aligned} \quad [1]$$

Here, $HU_{\varnothing}(x)$ was the HU value at voxel x and φ was the 4DCT phase bin (T00, T10, … , T90). L is the binary lung mask defined on each phase CT. As indicated in Eq. [1], all phases of 4DCT and the corresponding binary lung masks are required.

For the convenience of clinical use with less input requirement and faster calculation speed, we proposed a simplified algorithm, which only required average CT and the corresponding binary lung mask (36):

$$CTVI_{HU}(x) = \begin{cases} \dfrac{HU_{AVE}(X)}{-1000}\times\dfrac{HU_{AVE}(X)+1000}{1000} & if\ x\in L_{AVE} \\ 0 & if\ x\notin L_{AVE} \end{cases} \quad [2]$$

here $HU_{AVG}(x)$ and L_{AVG} are the HU value at voxel x and the binary lung mask defined on average CT, respectively.

Dose-volume metric and dose-function metric

Dose-volume metrics was calculated from the 3D dose

distribution based on average CT (planning CT). For each patient, dose-volume histogram (DVH) and mean lung dose (MLD) were calculated. The lung dose index Vx is defined as the percentage volume of lung receiving dose more than x Gy. For x =1 Gy, ..., 60 Gy, the values of Vx were calculated from DVH. The indexes of Vx and MLD jointly formed a one-dimensional feature vector with length of 61 for each patient.

Dose-function metrics was calculated from the 3D dose distribution and 4DCT-based VI. Using methods proposed for perfusion imaging (6), dose-function histograms (DFHs) was calculated by replacing volume with ventilation-based function. The functional MLD (fMLD) was calculated by weighting each dose voxel by its ventilation value. The functional Vx (fVx) is defined as the percentage ventilation function of lung receiving dose more than x Gy. For x = 1 Gy, ..., 60 Gy, the values of fVx were calculated from DFH. The indexes of fVx and fMLD jointly formed another one-dimensional feature vector with length of 61 for each patient.

The structure-based dose-volume feature vectors (MLD and Vxs) formed one set of samples, while the ventilation-based dose-function feature vectors (fMLD and fVxs) formed another set of samples. Both sets of feature vectors were first processed by PCA analysis. The few components with top-ranking were kept to represent the original feature space and the other components were discarded. PCA analysis reduced the dimensions of feature vector, which improved training efficiency and avoided overfitting of neural network.

Fuzzy clustering

The purpose of clustering is to identify natural groups of data from a large data set and produce a concise representation of a system's behavior. FCM (42) is a clustering technique that the degree of each data point belonging to a cluster is quantified by a membership grade. FCM is popularly used in pattern recognition and provided in many scientific software for engineers and researchers. In this study, we built our application based on FCM module of Fuzzy Logic Toolbox provided by MATLAB (The MathWorks, Natick, MA 01760, USA).

The objective function of the fuzzy clustering algorithm and its constraints are formulated as follows:

$$\min J(X,U,v_1,v_2,\cdots,v_k,\cdots,v_c)=\sum_{k=1}^{c}\sum_{i=1}^{N}\mu_{ki}^{m_0}d_{ki}^2 \qquad [3]$$

$$s.t.\begin{cases}\sum_{k=1}^{c}u_{ki}=1, & 1\le i\le N\\ u_{ki}\in[0,1], & 1\le k\le c, 1\le i\le N\\ \sum_{i=1}^{N}U_{ki}\in[0,N], & 1\le k\le c\end{cases} \qquad [4]$$

where N is the number of samples and C is the number of clustering centers. u_{ki} is the degree of membership indicating the degree to which the i-th sample belongs to the k-th class. U_{ki} is the membership matrix consisting of u_{ki}. The Euclidean distance d_{ki} is calculated by $\|v_k-x_i\|$. v_k is the k-th clustering center and m_0 is the fuzzy parameter. FCM starts with an initial guess for the cluster centers, which are intended to mark the mean location of each cluster. By Lagrange multiplier method, v_k and u_{ki} are determined as shown below.

$$v_k=\frac{\sum_{i=1}^{N}(\mu_{ki})m_0x_i}{\sum_{i=1}^{N}(\mu_{ki})m_0} \qquad [5]$$

$$u_{ki}=\frac{1}{\sum_{j=1}^{c}\left(\frac{d_{ki}}{d_{ji}}\right)^{\frac{2}{m_0-1}}} \qquad [6]$$

The initial guess for these cluster centers is most likely random. FCM assigns every data point a membership grade for each cluster. By iteratively updating the cluster centers and the membership grades for each data point, FCM iteratively moves the cluster centers to the right location within a data set. This iteration is based on minimizing an objective function that represents the distance from any given data point to a cluster center weighted by that data point's membership grade. As a result, FCM outputs a list of cluster centers' locations and membership grades for each data point.

Neural network modeling

The prediction model was based on fuzzy clustering and feed-forward neural network. The algorithm is briefly described as follows:

(I) The dataset is divided into two groups for training and testing purposes.
(II) During the training phase, FCM is used to classify the training samples and divide them into c categories with certain similarity measures;
(III) For each cluster, a feed-forward neural network is

established based on the specified training samples within the cluster;

(IV) During the testing phase, the Euclidean distance between the test sample and the center of each cluster is calculated, and the cluster of testing sample belonging to is selected by the minimum distance;

(V) The neural network of the cluster is selected to predict the occurrence of RP using the test samples of the cluster.

The feed-forward neural network with 8 hidden layers of neurons was selected (37). The tan-sigmoid function was used as the output layer function to limit the network output range [–1, 1]. The network training and testing were conducted by using the leave-one-out (LOO) cross validation method. In the LOO method, one patient's data from the total data set is excluded from predicting the network performance. The network is trained using the remaining data and tested with that excluded patient's data. This method maximizes the data available for training and can test a predictive model for a limited dataset.

Statistical analysis

A five-fold cross-validation procedure was applied to the 244 cases. Each fold contains approximately 20% RP cases and 80% non-RP cases. Each fold was selected as the testing data, and the remaining four folds were used as training data. Averaging prediction accuracy on five folds leaded to the overall accuracy estimate of the proposed method. In each fold of cross-validation, three neural networks were created and trained. They are NN-61 (neural network with input of the original feature vector with the length of 61), NN-5 (neural network with input of the compressed feature vector with the length of 5 after PCA analysis) and FCNN (fuzzy clustering neural network with input of the compressed feature vector with the length of 5 after PCA analysis).

The performance of model was quantified in terms of sensitivity [TP/(TP+FN)], specificity [TN/(TN+FP)], where TP is true positive, TN is true negative, FP is false positive, and FN is false negative. In addition, to test the ability of the new ventilation-based dosimetric features, area under the curve (AUC) was determined from the receiver operating characteristic (ROC) analysis. Radiation pneumonitis of ≥ Grade 3 was represented by positive values, while Radiation pneumonitis of ≤ Grade 2 was represented by negative values. This analysis was performed using R language (www.r-project.org) version 4.0. Student's *t*-test was used to compare the performance between predictive models built on structure-based and ventilation-based dosimetric features. The performance among NN-61, NN-5, and FCNN were evaluated for the effect of PCA and FCM. Statistical significance was defined as $P<0.05$.

Results

The patient cohort was composed of a heterogeneous population with a median age of 60.6 years (range, 35–79 years). The prescription dose ranged from 50 to 66 Gy, and the median follow-up duration was 18 months (range, 6–48 months). RP of Grade 2 or above was observed in 49 patients: 18 patients with Grade 2 pneumonitis, 29 patients with Grade 3, 0 patient with Grade 4, and 2 patients with Grade 5. The remaining 195 patients had Grade 1 RP. In this study, there was no significant correlation between RP (Grade ≥2) and pre-therapeutic lung disease, infectious lung disease after therapy or systemic therapy during and after radiation therapy.

A visual comparison between different VI is illustrated in *Figure 1* for a specific patient in transverse (first row) and coronal (second row) views. The correctness of the segmentation algorithm used in this study can be confirmed by comparing the original VI-SPECT (first column) and the segmented VI-SPECT (second column). The resulting 4DCT VI by the density-based algorithm (27), the Jacobian-based algorithm (28), the regional-based algorithm (29), and the simplified regional-based algorithm (36) are represented by CTVI-HU, CTVI-JAC, CTVI-PRO, and CTVI-AVG, respectively. In general, CTVI-PRO and CTVI-AVG were more similar to VI-SPECT. CTVI-HU and CTVI-JAC were less similar to VI-SPECT, especially in the regions as indicated by the yellow arrows.

The contribution rates of the top 5 principal components of the structure-based dosimetric features were 69.5, 19.9, 6.4, 1.8, and 0.8, while their values of the ventilation-based dosimetric features were 67.5, 21.2, 6.3, 2.1, and 1.0. The cumulative contribution rate of the top 2 principle components for both structure-based and ventilation-based dosimetric features were 89.4 and 88.7, respectively. Similarly, the cumulative contribution rate of the top 3 principle components for both structure-based and ventilation-based dosimetric features were 95.9 and 95.1, respectively. The cumulative contribution rate increased quickly when a few top-ranked principle components were added, and this increase slowed when more than 5 top-

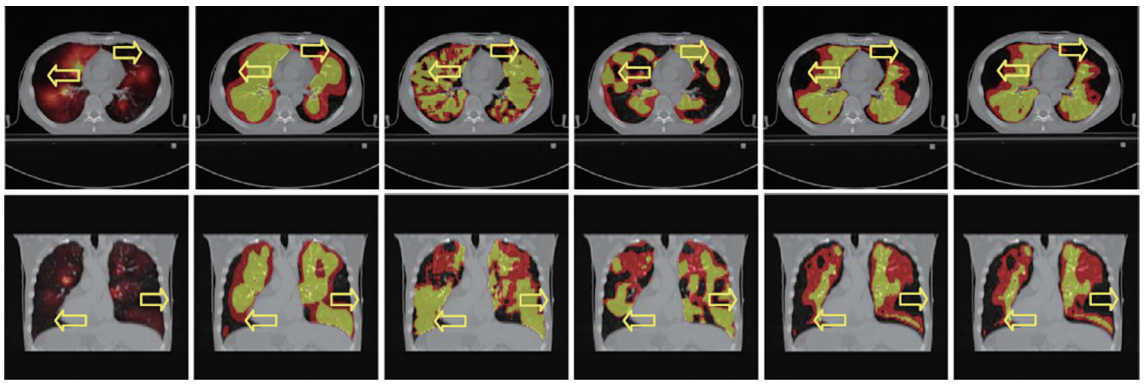

Figure 1 A comparison of the ventilation images generated by different algorithms. VI-SPECT, ventilation image generated by single photon emission computed tomography; CTVIHU, ventilation image generated by the density-based algorithm; CTVIJAC, ventilation image generated by the Jacobian-based algorithm; CTVI-PRO, ventilation image generated by the regional-based algorithm; CTVIAVG, ventilation image generated by the simplified regional-based algorithm.

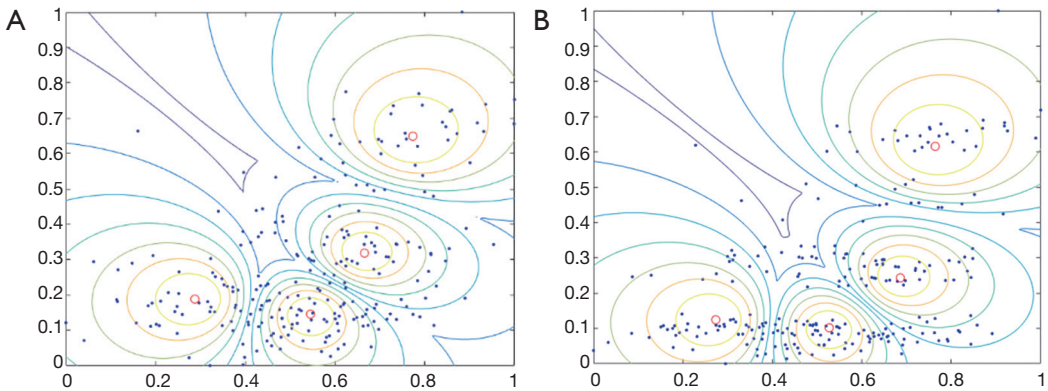

Figure 2 The projections of feature vectors on four clusters in two-dimensional principal component space. (A) The distribution of structure-based dosimetric feature vectors in 2D space; (B) the distribution of ventilation-based dosimetric feature vectors in 2D space.

ranked principle components were added. For balancing the efficiency and accuracy of the predictive model, the 5 top-ranked principle components were selected as dosimetric features. The cumulative contribution rate of the 5 top-ranked principle components for both structure-based and ventilation-based dosimetric features were 98.5 and 98.2, respectively, which is sufficient to represent the main feature information of the input data.

The determination of clustering number is another problem, which should be solved by validity evaluation criteria. In this study, several clustering validity indexes were tested, including SIL, DB, CH, BIC, and DUNN (43). The optimal number of clusters is 4 based on the tested indexes. *Figure 2* shows the result of FCM while the feature vectors of the samples were projected onto two-dimensional principal component space. The clusters of structure-based and ventilation-based feature vectors are comparatively shown in *Figure 2A*,*2B*. In each figure, the red circle represents the cluster center and the contour lines represent the membership relationship between the data point and the cluster. The x-axis is the first principal component score after normalization, and the y-axis is the second principal component score. It is noted that the cluster centers in both figures are similar, which implies that both types of dosimetric features may be highly correlated.

Figure 3 shows the ROC curves of the NN-61 tested on the structure-based and ventilation-based datasets. The AUC of the NN-61 using the structure-based dataset was 0.63, with sensitivity and specificity of 0.43 and 0.68, respectively. The AUC of the NN-61 using the ventilation-

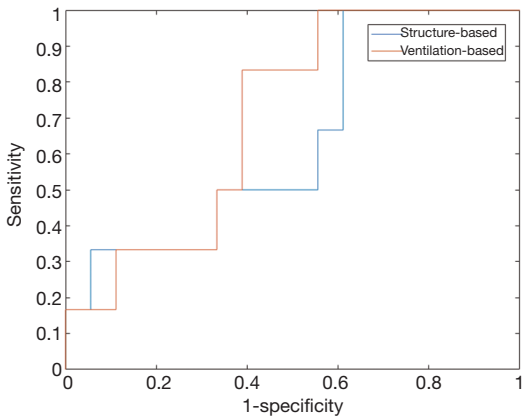

Figure 3 Receiver operating characteristic (ROC) curves of NN-61 using structure-based dosimetric features and ventilation-based dosimetric features.

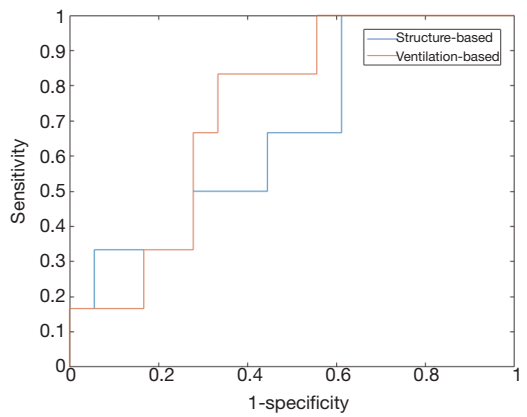

Figure 4 Receiver operating characteristic (ROC) curves of NN-5 using structure-based dosimetric features and ventilation-based dosimetric features.

based dataset was 0.70, with sensitivity and specificity of 0.53 and 0.69, respectively. The prediction accuracy of neural network using the ventilation-based is higher than that of the neural network using structure-based dosimetric features. The prediction capability of the network is significantly improved by using ventilation-based dosimetric features (P=0.016).

Figure 4 shows the ROC curves of the NN-5 tested on the structure-based and ventilation-based datasets. The AUC of the NN-5 on the structure-based dataset was 0.65, with sensitivity and specificity of 0.52 and 0.74, respectively. The AUC of the NN-5 on the ventilation-based dataset was 0.73, with sensitivity and specificity of 0.61

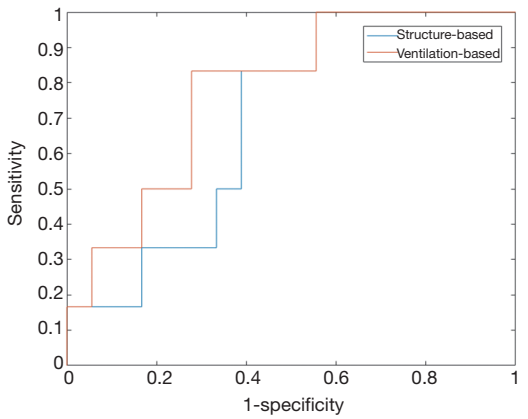

Figure 5 Receiver operating characteristic (ROC) curves of FCNN using structure-based dosimetric features and ventilation-based dosimetric features.

and 0.73, respectively. The prediction accuracy of neural network using the ventilation-based is higher than that of neural network using structure-based dosimetric features. The prediction capability of the network was significantly improved by using ventilation-based dosimetric features (P=0.015).

Figure 5 shows the ROC curves of the FCNN on the structure-based and ventilation-based datasets. The AUC of the FCNN on the structure-based dataset was 0.67, with sensitivity and specificity of 0.58 and 0.70, respectively. The AUC of the FCNN on the ventilation-based dataset was 0.77, with sensitivity and specificity of 0.71 and 0.76, respectively. The prediction accuracy of neural network using the ventilation-based is higher than that of neural network using structure-based dosimetric features. The prediction capability of the network was significantly improved by using ventilation-based dosimetric features (P=0.018).

Table 1 summarizes the AUC, sensitivity, and specificity of the networks NN-61, NN-5, and FCNN tested on the structure-based and ventilation-based datasets. Sensitivity and specificity were defined as the correctly predicted fraction of cases with and without RP, respectively. The average AUCs for both types of dosimetric features for NN-61 and NN-5 were 0.66 and 0.69, respectively. The prediction capability of the neural network was significantly improved by using PCA (P=0.022). The average AUCs for both types of dosimetric features for NN-5 and FCNN were 0.69 and 0.72, respectively. The prediction capability of the neural network was significantly improved by using

Table 1 A comparison of the NN-61, NN-5, and FCNN using structure-based dosimetric features and ventilation-based dosimetric features

Statistics	Structure-based dosimetric parameters			Ventilation-based dosimetric parameters		
	NN-61	NN-5	FCNN	NN-61	NN-5	FCNN
AUC	0.63	0.65	0.67	0.70	0.73	0.77
Sensitivity	0.43	0.52	0.58	0.53	0.61	0.71
Specificity	0.68	0.74	0.70	0.69	0.73	0.76

AUC, area under the curve.

FCM (P=0.025). The average AUCs of both types of dosimetric features for NN-61 and FCNN were 0.66 and 0.72, respectively. The prediction capability of the neural network was significantly improved by using both PCA and FCM (P=0.017).

Discussion

Current clinical methods used to predict the occurrence probability of RP are usually based on empirical thresholds. It is generally assumed that the lung is a homogenous tissue with the same radiotherapy response and RP can be predicted by clinically associated volume dose (V5, V10, V20, etc.) and the mean lung dose. However, there are two problems with this assumption. First, the lung volume is determined based on the instantaneous image. Since the lung volume of CT images obtained from different respiratory phases varies considerably, the accuracy of the dose volume of the lung could be affected considerably. Second, the ventilatory functions of different parts of the lung vary, especially in the lung affected by radiotherapy. The retrospective study showed that compared with the low ventilation function area before radiotherapy, the high ventilation function area had a more significant decline in carbon monoxide diffusion ability after irradiation. This finding suggests during treatment planning for thoracic patients, protecting the hyperventilation area can reduce lung injury and side effects after radiotherapy. It also showed that the dose in high ventilation lung areas could better predict RP. This study demonstrated that the average prediction accuracy and AUC value of classifiers using ventilation-based dosimetric features were higher than those of classifiers using structure-based dosimetric features. This further suggested that ventilation-based dosimetric features are more effective than those of structure-based dosimetric features for RP prediction.

The FCM algorithm was evolved from the K-means clustering algorithm. The algorithm's objective function is constructed based on the least mean square error function in the class. The essence of FCM is to get the membership degree of each sample point to the class centers by optimizing the objective function, so as to determine the class of the sample and achieve the automatic classification of the sample data set. However, the FCM algorithm has certain drawbacks. First, before clustering, the number of categories must be known in advance. In the case of prior knowledge (i.e., the number of categories is known), the objective function of the FCM algorithm can be calculated directly. However, in the case of unsupervised clustering, the number of clusters have to be determined in advance. Second, as a local search algorithm FCM is sensitive to the initial value. Randomly initializing the centroids or membership matrix will cause the algorithm to fall into the local optimum. There are several approaches to solve this problem. The Particle Swarm Optimization (PSO) algorithm can effectively avoid local minima. However, more time will be required for global random searching (44).

There are some limitations to this study. As shown in *Figure 2*, the clusters of samples are mapped onto two-dimensional space and the distance between the clusters is smaller. This implies that the samples in the new feature space might not be perfectly separated. Numerous reasons could cause this. First, the two principal components in the figure are 2 top-ranked principal components. Their cumulative contribution rate is about 88%, which does not fully represent the original feature space. Therefore, the distance of clusters in the two-dimensional feature space may differ from their actual distance in the five-dimensional feature space. Second, the definition of the objective function in the FCM algorithm depends on the choice of the distance measure. Different values of the objective functions could be obtained with different distance

measures. In this study, the Euclidean distance was used in the FCM algorithm. When the feature dimension is larger, the Euclidean distance might not be proper. Third, the size of the data set was limited. This current study required patients to conduct 4DCT imaging and therefore patients had to demonstrate high ventilation lung function before radiotherapy. These restrictions limited the enrolment of patients for this study. In the future, these restrictions should be relaxed by adopting 4D cone-beam CT (4DCBCT) instead of 4DCT and including patients with moderate ventilation lung function to expand our data set.

Conclusions

4DCT-VI provided by the simplified regional-based algorithm was more accurate and computationally more efficient at quantifying lung function compared to the original algorithm. The prediction accuracy of the neural network using ventilation-based dose-function metrics was higher than that of the traditional feed-forward neural network using structure-based dose-volume metrics. Together with the hybrid neural network, the ventilation-based dose-function metrics provided a promising and effective predictive model for RP.

Acknowledgments

Funding: This work is supported by the Natural Science Foundation of China (No.81502649, No. 11975312, No.11905295), Beijing Municipal Natural Science Foundation (No.7202170).

Footnote

Provenance and Peer Review: With the arrangement by the Guest Editors and the editorial office, this article has been reviewed by external peers.

Conflicts of Interest: All authors have completed the ICMJE uniform disclosure form (available at http://dx.doi.org/10.21037/qims-20-1095). The special issue "Artificial Intelligence for Image-guided Radiation Therapy" was commissioned by the editorial office without any funding or sponsorship. JD served as the unpaid Guest Editor of the special issue. The authors have no other conflicts of interest to declare.

Ethical Statement: The authors are accountable for all aspects of the work in ensuring that questions related to the accuracy or integrity of any part of the work are appropriately investigated and resolved. This study was approved by the institutional Ethics Committee of Cancer Hospital, Chinese Academy of Medical Sciences and Peking Union Medical College. Informed consent was waived in this retrospective study.

References

1. Kimura T, Togami T, Takashima H, Nishiyama Y, Ohkawa M, Nagata Y. Radiation pneumonitis in patients with lung and mediastinal tumours: a retrospective study of risk factors focused on pulmonary emphysema. Br J Radiol 2012;85:135-41.
2. Matsuoka S, Kurihara Y, Yagihashi K, Hoshino M, Watanabe N, Nakajima Y. Quantitative assessment of air trapping in chronic obstructive pulmonary disease using inspiratory and expiratory volumetric MDCT. AJR Am J Roentgenol 2008;190:762-9.
3. Rancati T, Ceresoli GL, Gagliardi G, Schipani S, Cattaneo GM. Factors predicting radiation pneumonitis in lung cancer patients: a retrospective study. Radiother Oncol 2003;67:275-83.
4. Kong FM, Hayman JA, Griffith KA, Kalemkerian GP, Arenberg D, Lyons S, Turrisi A, Lichter A, Fraass B, Eisbruch A, Lawrence TS, Ten Haken R. Final toxicity results of a radiation-dose escalation study in patients with non-small-cell lung cancer (NSCLC): predictors for radiation pneumonitis and fibrosis. Int J Radiat Oncol Biol Phys 2006;65:1075-86.
5. Marks LB, Bentzen SM, Deasy JO, Kong FM, Bradley JD, Vogelius IS, El Naqa I, Hubbs JL, Lebesque JV, Timmerman RD, Martel MK, Jackson AK. Radiation dose-volume effects in the lung. Int J Radiat Oncol Biol Phys 2010;76:S70-6.
6. Marks LB, Sherouse GW, Munley MT, Bentel GC, Spencer DP. Incorporation of functional status into dose-volume analysis. Med Phys 1999;26:196-9.

7. Graham MV, Purdy JA, Emami B, Harms W, Bosch W, Lockett MA, Perez CA. Clinical dose-volume histogram analysis for pneumonitis after 3D treatment for non-small cell lung cancer (NSCLC). Int J Radiat Oncol Biol Phys 1999;45:323-9.
8. Zhang XJ, Sun JG, Sun J, Ming H, Wang XX, Wu L, Chen ZT. Prediction of radiation pneumonitis in lung cancer patients: a systematic review. J Cancer Res Clin Oncol 2012;138:2103-16.
9. Nioutsikou E, Partridge M, Bedford JL, Webb S. Prediction of radiationinduced normal tissue complications in radiotherapy using functional image data. Phys Med Biol 2005;50:1035-46.
10. Rodrigues G, Lock M, D'Souza D, Yu E, Van Dyk J. Prediction of radiation pneumonitis by dose - volume histogram parameters in lung cancer-a systematic review. Radiother Oncol 2004;71:127-38.
11. McGuire SM, Zhou S, Marks LB, Dewhirst M, Yin FF, Das SK. A methodology for using SPECT to reduce intensity-modulated radiation therapy (IMRT) dose to functioning lung. Int J Radiat Oncol Biol Phys 2006;66:1543-52.
12. Siva S, Thomas R, Callahan J, Hardcastle N, Pham D, Kron T, Hicks RJ, MacManus MP, Ball DL, Hofman MS. High-resolution pulmonary ventilation and perfusion PET/CT allows for functionally adapted intensity modulated radiotherapy in lung cancer. Radiother Oncol 2015;115:157-62.
13. Ireland RH, Bragg CM, McJury M, Woodhouse N, Fichele S, van Beek EJ, Wild JM, Hatton MQ. Feasibility of image registration and IMRT planning with hyperpolarized helium-3 magnetic resonance imaging for non-small-cell lung cancer. Int J Radiat Oncol Biol Phys 2007;68:273-81.
14. Vinogradskiy Y, Castillo R, Castillo E, Tucker SL, Liao Z, Guerrero T, Martel MK. Use of 4-dimensional computed tomography-based ventilation imaging to correlate lung dose and function with clinical outcomes. Int J Radiat Oncol Biol Phys 2013;86:366-71.
15. Kadoya N, Cho SY, Kanai T, Onozato Y, Ito K, Dobashi S, Yamamoto T, Umezawa R, Matsushita H, Takeda K, Jingu K. Dosimetric impact of 4-dimensional computed tomography ventilation imaging-based functional treatment planning for stereotactic body radiation therapy with 3-dimensional conformal radiation therapy. Pract Radiat Oncol 2015;5:e505-12.
16. Ireland RH, Tahir BA, Wild JM, Lee CE, Hatton MQ. Functional Image-guided Radiotherapy Planning for Normal Lung Avoidance. Clin Oncol (R Coll Radiol) 2016;28:695-707.
17. Yamamoto T, Kabus S, Klinder T, Lorenz C, von Berg J, Blaffert T, Loo BW Jr, Keall PJ. Investigation of four-dimensional computed tomography-based pulmonary ventilation imaging in patients with emphysematous lung regions. Phys Med Biol 2011;56:2279-98.
18. Ding K, Bayouth JE, Buatti JM, Christensen GE, Reinhardt JM, et al. 4DCT-based measurement of changes in pulmonary function following a course of radiation therapy. Med Phys 2010;37:1261-72.
19. King MT, Maxim PG, Diehn M, Loo BW Jr, Xing L. Analysis of long-term 4-dimensional computed tomography regional ventilation after radiation therapy. Int J Radiat Oncol Biol Phys 2015;92:683-90.
20. Kipritidis J, Hugo G, Weiss E, Williamson J, Keall PJ. Measuring interfraction and intrafraction lung function changes during radiation therapy using four-dimensional cone beam CT ventilation imaging. Med Phys 2015;42:1255-67.
21. Kimura T, Doi Y, Nakashima T, Imano N, Kawabata H, Nishibuchi I, Okabe T, Kenjo M, Ozawa S, Murakami Y, Nagata Y. Combined ventilation and perfusion imaging correlates with the dosimetric parameters of radiation pneumonitis in radiation therapy planning for lung cancer. Int J Radiat Oncol Biol Phys 2015;93:778-87.
22. Yaremko BP, Guerrero TM, Noyola-Martinez J, Guerra R, Lege DG, Nguyen LT, Balter PA, Cox JD, Komaki R. Reduction of normal lung irradiation in locally advanced non-small-cell lung cancer patients, using ventilation images for functional avoidance. Int J Radiat Oncol Biol Phys 2007;68:562-71.
23. Yamamoto T, Kabus S, von Berg J, Lorenz C, Keall PJ. Impact of four-dimensional computed tomography pulmonary ventilation imaging-based functional avoidance for lung cancer radiotherapy. Int J Radiat Oncol Biol Phys 2011;79:279-88.
24. Kimura T, Nishibuchi I, Murakami Y, Kenjo M, Kaneyasu Y, Nagata Y. Functional image-guided radiotherapy planning in respiratory-gated intensity-modulated radiotherapy for lung cancer patients with chronic obstructive pulmonary disease. Int J Radiat Oncol Biol Phys 2012;82:e663-70.
25. Huang TC, Hsiao CY, Chien CR, Liang JA, Shih TC, Zhang GG. IMRT treatment plans and functional planning with functional lung imaging from 4D-CT for thoracic cancer patients. Radiat Oncol 2013;8:3.
26. Kida S, Bal M, Kabus S, Negahdar M, Shan X, Loo BW Jr, Keall PJ, Yamamoto T. CT ventilation functional image-based IMRT treatment plans are comparable to SPECT ventilation functional image-based plans. Radiother Oncol

2016;118:521-7.
27. Guerrero T, Sanders K, Castillo E, Zhang Y, Bidaut L, Pan T, Komaki R. Dynamic ventilation imaging from four-dimensional computed tomography. Phys Med Biol 2006;51:777-91.
28. Reinhardt JM, Ding K, Cao K, Christensen GE, Hoffman EA, Bodas SV. Registration-based estimates of local lung tissue expansion compared to xenon CT measures of specific ventilation. Med Image Anal 2008;12:752-63.
29. Kipritidis J, Hofman MS, Siva S, Callahan J, Le Roux PY, Woodruff HC, Counter WB, Keall PJ. Estimating lung ventilation directly from 4D CT Hounsfield unit values. Med Phys 2016;43:33.
30. Suga K. Technical and analytical advances in pulmonary ventilation SPECT with xenon-133 gas and Tc-99m-Technegas. Ann Nucl Med 2002;16:303-10.
31. Callahan J, Hofman MS, Siva S, Kron T, Schneider ME, Binns D, Eu P, Hicks RJ. High-resolution imaging of pulmonary ventilation and perfusion with 68Ga-VQ respiratory gated (4-D) PET/CT. Eur J Nucl Med Mol Imaging 2014;41:343-9.
32. Kipritidis J, Siva S, Hofman MS, Callahan J, Hicks RJ, Keall PJ. Validating and improving CT ventilation imaging by correlating with ventilation 4D-PET/CT using 68Ga-labeled nanoparticles. Med Phys 2014;41:011910.
33. Faught AM, Yamamoto T, Castillo R, Castillo E, Zhang J, Miften M, Vinogradskiy Y. Evaluating Which Dose-Function Metrics Are Most Critical for Functional-Guided Radiation Therapy. Int J Radiat Oncol Biol Phys 2017;99:202-9.
34. Otsuka M, Monzen H, Matsumoto K, Tamura M, Inada M, Kadoya N, Nishimura Y. Evaluation of lung toxicity risk with computed tomography ventilation image for thoracic cancer patients. PLoS One 2018;13:e0204721.
35. Siva S, Hardcastle N, Kron T, Bressel M, Callahan J, MacManus MP, Shaw M, Plumridge N, Hicks RJ, Steinfort D, Ball DL, Hofman MS. Ventilation/Perfusion Positron Emission Tomography-Based Assessment of Radiation Injury to Lung. Int J Radiat Oncol Biol Phys 2015;93:408-17.
36. Tian Y, Miao J, Liu Z, Huang P, Wang W, Wang X, Zhai Y, Wang J, Li M, Ma P, Zhang K, Yan H, Dai J. Availability of a simplified lung ventilation imaging algorithm based on four-dimensional computed tomography. Phys Med 2019;65:53-8.
37. Su M, Miften M, Whiddon C, Sun X, Light K, Marks L. An artificial neural network for predicting the incidence of radiation pneumonitis. Med Phys 2005;32:318-25.
38. Chen S, Zhou S, Zhang J, Yin FF, Marks LB, Das SK. A neural network model to predict lung radiation-induced pneumonitis. Med Phys 2007;34:3420-7.
39. Valdes G, Solberg TD, Heskel M, Ungar L, Simone CB. Using machine learning to predict radiation pneumonitis in patients with stage I non-small cell lung cancer treated with stereotactic body radiation therapy. Phys Med Biol 2016;61:6105-20.
40. Zhao Zheng, Morstatter F, Sharma S, Alelyani S, Anand A, Liu Huan. Advancing feature selection research. ASU Feature Selection Repository Arizona State University. 2010; 1-28.
41. De Sanctis R, Viganò A, Giuliani A, Gronchi A, De Paoli A, Navarria P, Quagliuolo V, Santoro A, Colosimo A. Unsupervised versus Supervised Identification of Prognostic Factors in Patients with Localized Retroperitoneal Sarcoma: A Data Clustering and Mahalanobis Distance Approach. Biomed Res Int 2018;2018:2786163.
42. Zhou H, Schaefer G, Shi C. Fuzzy C-Means Techniques for Medical Image Segmentation, Fuzzy Systems in Bioinformatics and Computational Biology, 2009;242:257-71.
43. Eréndira Rendón, Itzel M. Abundez, Citlalih Gutierrez, Sergio Díaz Zagal, Alejandra Arizmendi, Elvia M. Quiroz, and H. Elsa Arzate. A comparison of internal and external cluster validation indexes. Proceedings of the 2011 American conference on applied mathematics and the 5th WSEAS international conference on Computer engineering and applications, 2011, 158-63.
44. Mekhmoukh A, Mokrani K. Improved Fuzzy C-Means based Particle Swarm Optimization (PSO) initialization and outlier rejection with level set methods for MR brain image segmentation. Comput Methods Programs Biomed 2015;122:266-81.

Cite this article as: Huang P, Yan H, Hu Z, Liu Z, Tian Y, Dai J. Predicting radiation pneumonitis with fuzzy clustering neural network using 4DCT ventilation image based dosimetric parameters. Quant Imaging Med Surg 2021;11(12):4731-4741. doi: 10.21037/qims-20-1095

